

Determination of the Heart-to-Mediastinum Ratio of ^{123}I -MIBG Uptake Using Dual-Isotope (^{123}I -MIBG/ $^{99\text{m}}\text{Tc}$ -Tetrofosmin) Multipinhole Cadmium-Zinc-Telluride SPECT in Patients with Heart Failure

Tanguy Blaire^{1–3}, Alban Bailliez^{1–3}, Fayçal Ben Bouallegue⁴, Dimitri Bellevre⁵, Denis Agostini^{2,5}, and Alain Manrique^{2,5}

¹Department of Nuclear Medicine, UF 5881, Groupement des Hôpitaux de l'Institut Catholique de Lille, Lomme, France;

²Signalisation, Électrophysiologie et Imagerie des Lésions d'Ischémie-Reperfusion Myocardique, UNICAEN, Normandie Université, Caen, France; ³Department of Nuclear Medicine, IRIS, Polyclinique du Bois, Lille, France; ⁴Department of Nuclear Medicine, CHU de Montpellier, Montpellier, France; and ⁵Department of Nuclear Medicine, CHU Cote de Nacre, Caen, France

The aim of this retrospective study was to compare the heart-to-mediastinum ratio (HMR) of ^{123}I -metaiodobenzylguanidine (^{123}I -MIBG) uptake obtained using a multipinhole cadmium-zinc-telluride (CZT) camera with that obtained using conventional planar imaging.

Methods: Forty consecutive heart failure patients underwent planar acquisition 4 h after ^{123}I -MIBG injection (191 ± 41 [mean \pm SD] MBq). To localize the heart using the CZT camera, $^{99\text{m}}\text{Tc}$ -tetrofosmin (358 ± 177 MBq) was administered and dual-isotope acquisition was performed. The HMRs were calculated with conventional planar imaging ($\text{HMR}_{\text{planar}}$), with anterior reprojection images using the CZT camera ($\text{HMR}_{\text{reproj}}$), and with transaxial reconstructed images using the CZT camera ($\text{HMR}_{\text{transaxial}}$). In a phantom study, we estimated a linear model fitting the CZT camera data to the planar data, and we applied it to provide corrected CZT camera-determined HMRs in patients ($\text{cHMR}_{\text{reproj}}$ and $\text{cHMR}_{\text{transaxial}}$).

Results: Thirty-four men and 6 women (71 ± 9 y old) with ischemic (22 patients) and nonischemic (18 patients) heart failure completed the study. For 22 of the 40 patients (55%), the New York Heart Association classification was class II and the ejection fraction was $35\% \pm 9\%$. $\text{HMR}_{\text{reproj}}$ (1.12 ± 0.19) and $\text{HMR}_{\text{transaxial}}$ (1.35 ± 0.34) were lower than $\text{HMR}_{\text{planar}}$ (1.44 ± 0.14) ($P < 0.0001$ and $P < 0.01$, respectively). $\text{cHMR}_{\text{reproj}}$ (1.54 ± 0.09) and $\text{cHMR}_{\text{transaxial}}$ (1.45 ± 0.14) were significantly different ($P < 0.0001$). Lin concordance correlation and Bland-Altman analysis demonstrated an almost perfect concordance and a high agreement between $\text{HMR}_{\text{planar}}$ and $\text{cHMR}_{\text{transaxial}}$ (P was not significant) but not between $\text{HMR}_{\text{planar}}$ and $\text{cHMR}_{\text{reproj}}$ ($P < 0.0001$).

Conclusion: This study demonstrated that determination of the late HMR of cardiac ^{123}I -MIBG uptake using dual-isotope (^{123}I and $^{99\text{m}}\text{Tc}$) acquisition on a multipinhole CZT camera was feasible in patients with heart failure. However, this determination should be performed using transaxial reconstructed images and linear correction based on phantom data acquisitions.

Key Words: CZT; DNM-530c; ^{123}I -MIBG; heart-to-mediastinum ratio; heart failure; dual isotopes

J Nucl Med 2018; 59:251–258

DOI: 10.2967/jnumed.117.194373

Impairment of cardiac sympathetic innervation assessed with ^{123}I -metaiodobenzylguanidine (^{123}I -MIBG) has been recognized as an independent prognostic factor in patients with heart failure (1–6). The late heart-to-mediastinum ratio (HMR) of ^{123}I -MIBG is a major predictor of sudden death and cardiac events in patients with heart failure. An HMR of less than 1.6 is associated with an increased risk (6). At present, calculation of the HMR requires a planar static image of the thorax. This technique is well standardized and reproducible using a conventional Anger camera (7,8). Recently, dedicated cardiac SPECT cameras using cadmium-zinc-telluride (CZT) detectors dramatically transformed the routine of myocardial perfusion imaging in patients with known or suspected coronary artery disease. These cameras have a better count detection sensitivity, resulting in decreased acquisition times and injected radiopharmaceutical doses, and improved energy resolution, permitting better photon energy discrimination for dual-isotope imaging.

Myocardial perfusion imaging obtained using cardiac CZT cameras has been well validated against that obtained using the conventional Anger camera for the diagnosis of coronary artery disease (9–12). Only a few studies have evaluated myocardial sympathetic innervation imaging with these new-generation detectors (13–16). With the Discovery NM 530c (DNM-530c; GE Healthcare), Gimelli et al. (13,14) assessed regional left ventricular denervation. D'estanque et al. (15) reported the impact of scatter correction in dual-isotope ($^{201}\text{Tl}/^{123}\text{I}$ -MIBG) cardiac SPECT protocols for the assessment of trigger zones, defined as areas of autonomic nervous system dysfunction in viable myocardium that may contribute to the genesis of ventricular arrhythmia. In the ADRECARD study, Bellevre et al. (16) recently demonstrated that determination of the late HMR of ^{123}I -MIBG uptake using a parallel-collimator CZT camera (DSPECT; Biosensors International) was feasible in patients with heart failure. The 2 commercially available CZT cameras differ in sensitivity (4-fold

Received Apr. 6, 2017; revision accepted Jun. 13, 2017.

For correspondence or reprints contact: Tanguy Blaire, Department of Nuclear Medicine, UF 5881, Groupement des Hôpitaux de l'Institut Catholique de Lille, Lomme, France.

E-mail: Blair.Tanguy@ghicl.net

Published online Jun. 23, 2017.

COPYRIGHT © 2018 by the Society of Nuclear Medicine and Molecular Imaging.

improved with DNM-530c and nearly 7-fold improved with DSPECT) and spatial resolution (6.7 mm with DNM-530c and 8.6 mm with DSPECT), leading to images with different degrees of sharpness and contrast-to-noise ratios (11,17,18).

Until now, there have been no reports on the use of the DNM-530c, a multipinhole CZT SPECT camera, for determination of the HMR of ^{123}I -MIBG uptake. As previously emphasized (19,20), quantification of the HMR is influenced by the type of collimators used and the number of scattered photons. Consequently, the value of the HMR is expected to depend on the type of CZT camera used. Hence, a study to validate the multipinhole dedicated cardiac CZT camera is needed.

The aim of this study was to compare the late HMR of ^{123}I -MIBG uptake determined using dual-isotope CZT acquisition (DNM-530c) with that determined using conventional planar imaging in patients with heart failure.

MATERIALS AND METHODS

Phantom Studies

To estimate the effectiveness of the DNM-530c camera in measuring the HMR, we performed several phantom acquisitions using an anthropomorphic torso phantom (Data Spectrum) with a cardiac insert. The liver and mediastinum compartments were filled with ^{123}I activities of 20 MBq (17.5 kBq/mL) and 5 MBq (0.6 kBq/mL), respectively. Ten consecutive acquisitions were performed over 10 min using a conventional Anger camera (Infinia; GE Healthcare) and a CZT camera (DNM-530c). The cardiac insert was repeatedly unloaded from 1.75 (11 kBq/mL) to 1.5, 1.25, 1.1, 0.94, 0.75, 0.5, 0.35, 0.25, and 0.1 MBq to obtain a wide range of HMRs of ^{123}I , as previously described (16,20).

Patient Population

All procedures in studies involving human participants were performed in accordance with the ethical standards of the institutional or national research committee and with the principles of the 1964 Declaration of Helsinki and its later amendments or comparable ethical standards. This retrospective study was approved by the Hospital Ethics Committee for Medical Research (CIER 03/01/2016). Informed written consent was obtained from all individual participants included in the study. Data from 40 consecutive patients who had clinically stable ischemic or nonischemic heart failure (left ventricular ejection fraction [LVEF], <45%) and were referred to our institution from May 2011 to May 2016 were retrospectively evaluated. Patients with a recent (<21 d) history of unstable angina or acute myocardial infarction were excluded from the study.

Conventional Anger Camera Protocol (Planar Imaging)

The imaging protocol (Fig. 1) was performed according to the recommendations of the EANM Cardiovascular Committee and the European Council of Nuclear Cardiology (7). ^{123}I -MIBG (191 ± 29 [mean \pm SD] MBq, depending on the patient's weight) was administered 30 min after blockade of the thyroid by oral administration of Lugol solution. Four hours after injection, a late planar image was first obtained on a conventional γ -camera system, a dual-head γ -camera (Infinia) equipped with low-energy high-resolution collimators. Planar images were acquired in the anterior view over 10 min (128×128 matrix) using a symmetric energy window (159 ± 10 keV).

Dual-Isotope (^{123}I -MIBG/ $^{99\text{m}}\text{Tc}$ -Tetrofosmin) CZT Acquisition Protocol (DNM-530c)

$^{99\text{m}}\text{Tc}$ -tetrofosmin (358 ± 177 MBq) was administered for myocardial perfusion imaging to localize the heart within the thorax. After

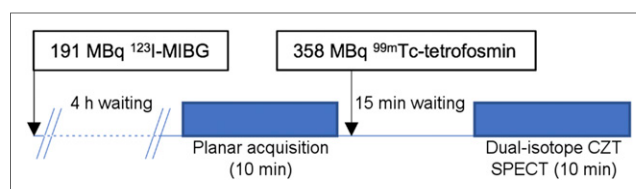


FIGURE 1. Imaging study protocol. First acquisition was single-isotope planar acquisition using conventional camera. Second acquisition was dual-isotope acquisition using CZT camera.

15 min, the $^{99\text{m}}\text{Tc}$ image helped focus the detectors on the cardiac area. A 10-min list-mode simultaneous dual-radionuclide ($^{99\text{m}}\text{Tc}$ and ^{123}I) gated scan was then performed using a dedicated cardiac CZT SPECT camera (DNM-530c). DNM-530c is equipped with 19 stationary CZT detectors, each equipped with a pinhole collimator, that simultaneously image 19 cardiac views; each detector is composed of four 5-mm-thick elements of 32×32 pixels (pixel size, 2.46×2.46 mm) (17). List-mode acquisition permits the retrospective selection of $^{99\text{m}}\text{Tc}$ and ^{123}I energy windows set to 140 keV (-10 to $+5\%$) and 159 keV (-5 to $+10\%$), respectively. No scatter correction was performed.

Previous studies using phantom data acquired separately for $^{99\text{m}}\text{Tc}$ and ^{123}I showed that $^{99\text{m}}\text{Tc}$ cross-talk into the ^{123}I window was negligible when a simultaneous CZT SPECT acquisition was performed (21,22). To ensure that different $^{99\text{m}}\text{Tc}/^{123}\text{I}$ ratios did not have an impact on energy resolution, we acquired a set of energy spectra (single ^{123}I , single $^{99\text{m}}\text{Tc}$, and dual $^{123}\text{I}/^{99\text{m}}\text{Tc}$) using linear sources with three $^{99\text{m}}\text{Tc}/^{123}\text{I}$ ratios (0.5:1, 1:1, and 5:1) and a constant activity of ^{123}I (24 MBq) (Fig. 2).

Analysis of HMR of ^{123}I -MIBG Uptake

The HMR was calculated from the planar images ($\text{HMR}_{\text{planar}}$). Myocardial and mediastinal counts were obtained by drawing regions of interest (ROIs) manually on the left ventricle and over the upper mediastinum area (7).

Using SPECT data, we tested 2 different methods for assessing the HMR of ^{123}I -MIBG uptake. First, the HMR was calculated with a reprojected anterior view of SPECT images reconstructed using the vendor's console ($\text{HMR}_{\text{reproj}}$). The reprojection of tomographic data assumed an ideal parallel-hole collimation and did not simulate attenuation or scatter. An ROI encompassing the left ventricle was drawn manually on the $^{99\text{m}}\text{Tc}$ -tetrofosmin images and automatically copied to the ^{123}I -MIBG images. A mediastinum ROI (42 pixels) was then drawn on the ^{123}I -MIBG images.

Second, the HMR was calculated with transaxial reconstructed SPECT images ($\text{HMR}_{\text{transaxial}}$). A myocardial elliptic volume of interest (VOI) was drawn manually to encompass the whole heart on the $^{99\text{m}}\text{Tc}$ -tetrofosmin images. This VOI was automatically copied from the $^{99\text{m}}\text{Tc}$ -tetrofosmin images to the ^{123}I -MIBG images. A mediastinum VOI (300 voxels) was manually drawn on the ^{123}I -MIBG images.

HMR Correction Factor

Many factors affecting the HMR of ^{123}I -MIBG uptake differed between the Infinia and DNM-530c cameras, including the type of collimator (parallel-hole low-energy high-resolution with Infinia vs. multipinhole with DNM-530c), energy window, energy resolution (which was better with DNM-530c [$\sim 9\%$ with Infinia vs. $\sim 5\%$ with DNM-530c]), and detector material stopping power (84% for 9.5-mm NaI(Tl) vs. 78% for 5-mm CZT for 159-keV photons). To take into account the difference between DNM-530c and Infinia, we applied to the HMR quantification a correction factor based on phantom acquisitions. To extract a correction factor from the analysis, we used a linear regression equation obtained in the phantom study. We calculated a corrected $\text{HMR}_{\text{reproj}}$ ($\text{cHMR}_{\text{reproj}}$) and a corrected $\text{HMR}_{\text{transaxial}}$

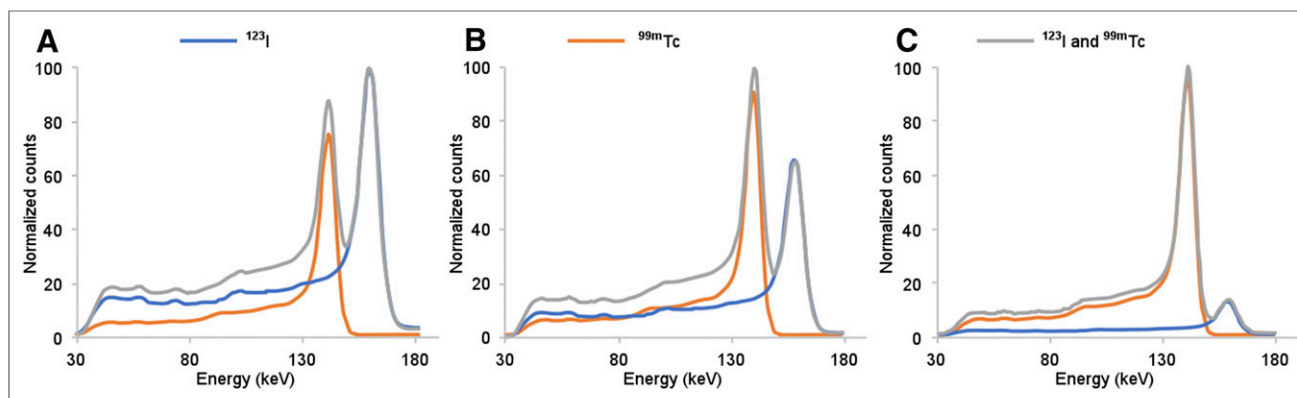


FIGURE 2. Single ^{123}I (24 MBq), single $^{99\text{m}}\text{Tc}$, and simultaneous (^{123}I and $^{99\text{m}}\text{Tc}$) energy spectra using linear sources and DNM-530c. Low tailing effect and downscatter of ^{123}I toward $^{99\text{m}}\text{Tc}$ (and absence of $^{99\text{m}}\text{Tc}$ scatter toward ^{123}I) were seen in dual-isotope condition, whatever the ratio of $^{99\text{m}}\text{Tc}$ activity to ^{123}I activity: 0.5:1 (A), 1:1 (B), or 5:1 (C).

($\text{cHMR}_{\text{transaxial}}$) for each patient in the validation group for further comparison with the $\text{HMR}_{\text{planar}}$ values (16,23).

LVEF $^{99\text{m}}\text{Tc}$ -Tetrofosmin SPECT with DNM-530c

As previously reported (22), the presence of ^{123}I did not have an impact on LVEF assessment within the $^{99\text{m}}\text{Tc}$ energy window in the dual-isotope condition for DNM-530c. Accordingly, the LVEF was assessed using Quantitative Gated SPECT software (Cedars-Sinai Medical Center).

Statistical Analysis

The normal distribution of data was tested with the Shapiro–Wilk test. Paired HMRs determined using Infinia and DNM-530c were compared using the Student *t* test for paired samples. Correlations among $\text{HMR}_{\text{planar}}$, $\text{HMR}_{\text{reproj}}$, and $\text{HMR}_{\text{transaxial}}$ were assessed using linear regression and Pearson correlation analysis. Concordance among $\text{HMR}_{\text{planar}}$, $\text{HMR}_{\text{reproj}}$, and $\text{HMR}_{\text{transaxial}}$ values was tested using the Lin concordance correlation coefficient (CCC) (24) and Bland–Altman analysis (25). The Lin CCC is essentially equivalent to the κ -coefficient but is applicable to continuous data. It evaluates both accuracy and precision, indicating how far measurement pairs are away from the line of identity. The Lin CCC scale ranges from 0 (no agreement) to +1 (perfect agreement), where 0.21–0.40 indicates fair concordance, 0.41–0.60 indicates moderate concordance, 0.61–0.80 indicates substantial concordance, and 0.81–0.99 indicates almost perfect concordance. A 2-tailed *P* value of less than or equal to 0.05 was considered statistically significant. Statistical analysis was performed using R version 3.3.2 (R Foundation for Statistical Computing).

RESULTS

Phantom Study

The HMRs obtained from the phantom acquisitions are shown in Table 1. $\text{HMR}_{\text{reproj}}$ (2.82 ± 1.5) and $\text{HMR}_{\text{transaxial}}$ (3.51 ± 1.94) were higher than $\text{HMR}_{\text{planar}}$ (2.34 ± 0.8) (*P* was not significant and *P* = 0.01, respectively). However, Bland–Altman plots demonstrated that $\text{HMR}_{\text{reproj}}$ and $\text{HMR}_{\text{transaxial}}$ were underestimated for low HMRs and overestimated for high HMRs. The corrections used for the calculation of $\text{cHMR}_{\text{reproj}}$ and $\text{cHMR}_{\text{transaxial}}$ were determined by linear regression between CZT and planar HMRs in the phantom study: $\text{cHMR}_{\text{reproj}} = 0.4715 \times \text{HMR}_{\text{reproj}} + 1.0416$ (*r* = 0.98) and $\text{cHMR}_{\text{transaxial}} = 0.4106 \times \text{HMR}_{\text{transaxial}} + 0.8987$ (*r* = 0.99), respectively.

Population

Among the 40 consecutive patients (34 men and 6 women; mean age, 71 ± 9 y; mean LVEF, $35\% \pm 9\%$) with heart failure included in the study, 22 (55%) had ischemic heart failure and 18 (45%) had nonischemic heart failure. Patient characteristics are shown in Table 2. The New York Heart Association functional classifications were class I for 13 patients, class II for 22 patients, and class III for 5 patients. End-diastolic and end-systolic volumes and LVEF obtained using $^{99\text{m}}\text{Tc}$ -tetrofosmin SPECT were 171 ± 87 mL, 117 ± 67 mL, and $36\% \pm 17\%$, respectively.

HMR Quantification in Patients: DNM-530c Versus Planar Imaging

In our population, $\text{HMR}_{\text{reproj}}$ (1.12 ± 0.19) and $\text{HMR}_{\text{transaxial}}$ (1.35 ± 0.34) were significantly lower than $\text{HMR}_{\text{planar}}$ (1.44 ± 0.14) (*P* < 0.0001 and *P* < 0.05, respectively). Figures 3A and 4A show the Lin CCCs between $\text{HMR}_{\text{reproj}}$ and $\text{HMR}_{\text{planar}}$ (Fig. 3A) and between $\text{HMR}_{\text{transaxial}}$ and $\text{HMR}_{\text{planar}}$ (Fig. 4A); these data demonstrated only a fair concordance between $\text{HMR}_{\text{reproj}}$ and

TABLE 1
HMRs from Phantom Acquisitions

Heart activity (MBq)	$\text{HMR}_{\text{planar}}$	$\text{HMR}_{\text{reproj}}$	$\text{HMR}_{\text{transaxial}}$
1.75	3.56	5.33	6.49
1.5	3.34	4.82	5.77
1.25	2.88	3.84	4.60
1.1	2.77	3.73	4.90
0.94	2.41	2.50	3.81
0.75	2.29	2.14	3.35
0.5	1.86	1.69	2.33
0.35	1.61	1.57	1.65
0.25	1.48	1.34	1.49
0.1	1.21	1.26	0.73
Mean \pm SD	2.34 ± 0.8	2.82 ± 1.5	3.51 ± 1.94

TABLE 2
Patient Characteristics

Patient	Age (y)	Sex	Heart failure	NYHA functional class	LVEF (%)	Administered dose (MBq)		HMR _{planar}	HMR _{reproj}	HMR _{transaxial}	cHMR _{reproj}	cHMR _{transaxial}
						¹²³ I-MIBG	^{99m} Tc-tetrofosmin					
1	70	M	ICM	II	36	196	241	1.54	1.23	1.48	1.6	1.51
2	67	M	ICM	III	20	181	222	1.41	1.12	1.36	1.55	1.46
3	65	F	NICM	II	30	151	264	1.23	0.83	0.88	1.41	1.26
4	77	M	NICM	I	44	125	370	1.38	0.96	1.2	1.48	1.4
5	82	M	NICM	I	44	181	265	1.35	1.04	0.99	1.51	1.31
6	67	M	ICM	II	32	206	282	1.37	0.85	1.18	1.42	1.38
7	79	M	ICM	I	34	212	245	1.53	1.38	1.42	1.68	1.48
8	75	M	ICM	II	33	199	109	1.41	1.21	1.17	1.59	1.38
9	73	M	ICM	II	45	204	632	1.48	1.02	1.47	1.5	1.51
10	78	M	ICM	I	44	186	271	1.39	1.09	1.52	1.54	1.53
11	67	M	NICM	II	40	154	734	1.54	1.13	1.6	1.56	1.56
12	81	M	NICM	II	40	183	276	1.36	1.0	1.5	1.49	1.52
13	69	F	NICM	I	40	192	578	1.48	1.12	1.47	1.55	1.51
14	85	M	ICM	I	40	212	225	1.56	1.1	1.68	1.54	1.59
15	78	M	ICM	I	45	200	176	1.0	0.48	0.22	1.24	0.99
16	64	M	NICM	III	20	189	232	1.57	1.28	1.78	1.63	1.63
17	76	M	ICM	I	36	189	525	1.63	1.18	1.73	1.58	1.61
18	58	M	NICM	III	24	125	370	1.36	1.06	1.02	1.52	1.32
19	70	M	NICM	II	35	119	880	1.63	1.6	1.84	1.79	1.66
20	59	M	ICM	I	35	221	290	1.35	1.00	1.02	1.49	1.32
21	60	M	ICM	II	31	193	549	1.32	0.98	0.97	1.48	1.3
22	82	M	NICM	II	32	175	528	1.65	1.17	1.89	1.58	1.68
23	55	M	NICM	II	35	204	263	1.53	1.26	1.52	1.62	1.52
24	70	M	ICM	II	35	196	288	1.28	0.92	1.23	1.45	1.41
25	77	M	NICM	III	29	191	225	1.48	1.03	1.38	1.51	1.47
26	80	M	ICM	II	30	223	267	1.35	1.06	1.04	1.52	1.33
27	68	M	ICM	II	35	152	263	1.37	1.11	1.36	1.55	1.46
28	80	M	ICM	II	30	188	302	1.32	1.2	1.26	1.59	1.42
29	67	M	NICM	II	33	199	335	1.48	1.22	1.37	1.6	1.47
30	71	M	ICM	II	35	216	308	1.31	0.99	1.11	1.49	1.36
31	70	M	ICM	II	40	214	275	1.26	1.19	1.1	1.58	1.35
32	70	F	NICM	II	33	197	597	1.42	1.09	1.39	1.53	1.47
33	72	F	ICM	I	33	222	235	1.64	1.08	1.74	1.53	1.62
34	54	M	ICM	II	30	181	317	1.44	1.33	1.24	1.65	1.41
35	59	F	NICM	I	42	206	326	1.28	0.91	1.02	1.45	1.32
36	60	F	NICM	I	45	205	377	1.57	1.1	1.69	1.54	1.6
37	72	M	NICM	III	20	247	295	1.45	1.2	1.11	1.59	1.36
38	77	M	NICM	II	32	225	345	1.47	1.06	1.29	1.52	1.43
39	59	M	ICM	II	40	174	294	1.69	1.48	1.95	1.73	1.7
40	59	M	ICM	I	40	198	720	1.57	1.38	1.67	1.68	1.59
Mean ± SD	71 ± 9				35 ± 9	191 ± 41	358 ± 177	1.44 ± 0.14	1.12 ± 0.19	1.35 ± 0.34	1.54 ± 0.09	1.45 ± 0.14

NYHA = New York Heart Association; ICM = ischemic; NICM = nonischemic.

HMR_{planar} (CCC, 0.24) but demonstrated a substantial concordance between HMR_{transaxial} and HMR_{planar} (CCC, 0.61). Bland–Altman plots (Figs. 3B and 4B) demonstrated a poor agreement between HMR_{reproj} and HMR_{planar} (Fig. 3B) and between HMR_{transaxial} and HMR_{planar} (Fig. 4B), leading to an underestimation of values by DNM-530c. Figure 5 shows Infinia and DNM-530c images.

HMR Quantification in Patients: Corrected DNM-530c Versus Planar Imaging

cHMR_{reproj} (1.54 \pm 0.09) but not cHMR_{transaxial} (1.45 \pm 0.14) was significantly higher than HMR_{planar} (1.44 \pm 0.14) (P < 0.0001 and P was not significant, respectively). As shown in Figure 3C, there was a moderate concordance between cHMR_{reproj}

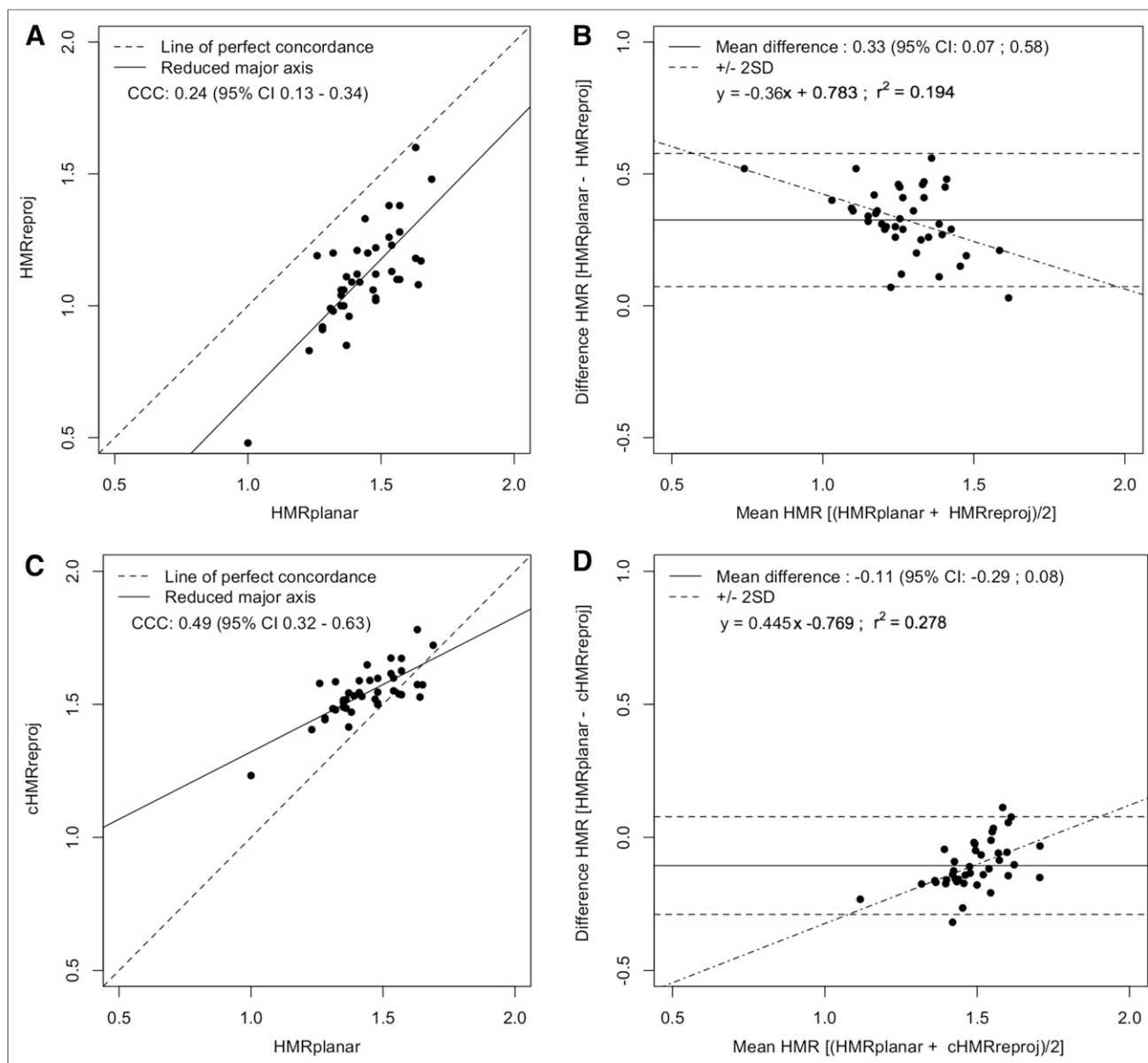


FIGURE 3. Lin CCC plots (A and C) and Bland–Altman plots (B and D) showing agreement between HMR_{reproj} and HMR_{planar} (A and B) and between cHMR_{reproj} and HMR_{planar} (C and D).

and HMR_{planar} (CCC, 0.49). Bland–Altman plots (Fig. 3D) showed a moderate agreement between cHMR_{reproj} and HMR_{planar}. The mean difference between the HMRs from the 2 techniques was 0.11, but the difference increased significantly as a function of the mean HMR value.

In contrast, as shown in Figure 4C, there was an almost perfect concordance between cHMR_{transaxial} and HMR_{planar} (CCC, 0.92). Bland–Altman plots (Fig. 4D) showed a high agreement between cHMR_{transaxial} and HMR_{planar}. The mean difference between the HMRs from the 2 techniques was 0.01, with a narrow 95% confidence interval, and was stable over the whole range of HMRs.

DISCUSSION

Late HMR determination using the Anger camera is well standardized, and its prognostic value is widely recognized. In

this retrospective study, we determined the HMR of ¹²³I-MIBG uptake using a multipinhole dedicated cardiac CZT camera (DNM-530c) in patients with heart failure and low LVEF. To our knowledge, this is the first dual-isotope study combining ¹²³I-MIBG and ^{99m}Tc-tetrofosmin with a multipinhole CZT camera to assess cardiac neuronal function in heart failure. Late HMRs (HMR_{reproj} and HMR_{transaxial}) in patients were significantly lower than HMR_{planar}, but the latter showed high agreement with cHMR_{transaxial}. Our results are consistent with findings from the ADRECARD study (16), which was conducted using another model of the dedicated cardiac CZT camera, with different spatial resolution and sensitivity (17,26).

Difference Between Planar and CZT SPECT HMRs

First, to better understand the camera responses in ¹²³I-MIBG imaging, we compared planar and DNM-530c phantom acquisitions

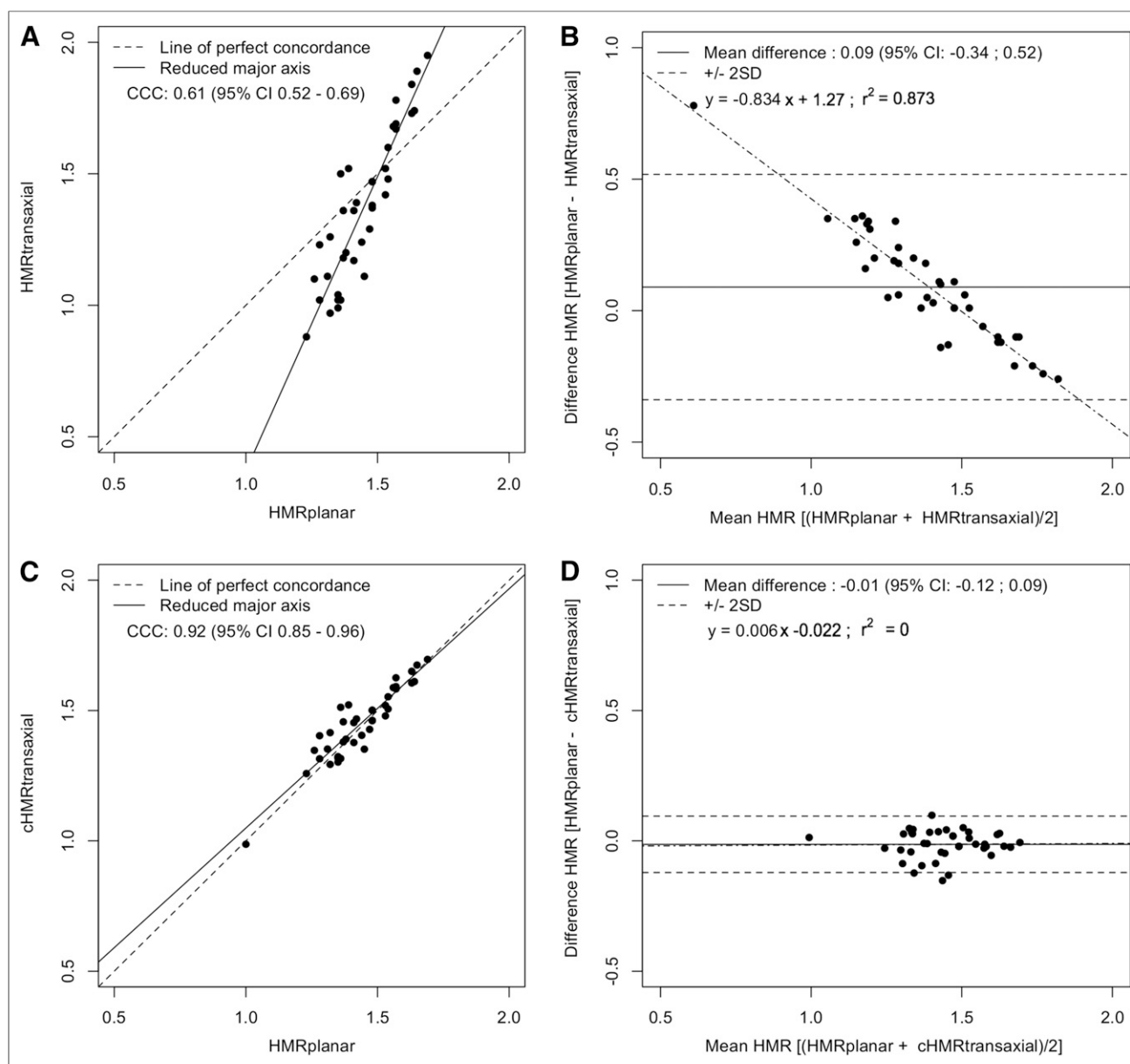


FIGURE 4. Lin CCC plots (A and C) and Bland-Altman plots (B and D) showing agreement between HMR_{transaxial} and HMR_{planar} (A and B) ($P < 0.01$) and between cHMR_{transaxial} and HMR_{planar} (C and D).

and found that the noncorrected HMRs obtained with DNM-530c underestimated low values and overestimated high values of ^{123}I -MIBG uptake. Accordingly, HMRs in patients were significantly lower with DNM-530c than with the Anger camera, as these patients with heart failure had decreased ^{123}I -MIBG uptake.

The collimators used and the stopping power of the detector material may have an impact on the quantification of the ^{123}I -MIBG HMR (20,27). Inoue et al. (23) found that a correction factor is necessary to improve exchangeability between HMRs calculated using medium-energy collimators and those calculated using low- to medium-energy collimators. Nakajima et al. (28–30) demonstrated that the linear regression equation for low-energy and medium-energy collimators in a phantom study can be used for standardizing the measurement of HMR in ^{123}I -MIBG imaging. In the present study, after correction, there was still a significant

difference between cHMR_{reproj} and HMR_{planar} ($P < 0.0001$), but there was no difference between cHMR_{transaxial} and HMR_{planar} (P was not significant).

Using a different model of camera with mobile CZT detector columns and parallel tungsten collimators (DSPECT), Bellevre et al. (16) extracted a planar equivalent image by projecting and summing all of the elementary 2-dimensional images that shared the same angle on 1 large-field-of-view virtual plane (16). After applying a similar correction based on linear regression between SPECT and planar phantom acquisitions, they found a high agreement between the ^{123}I -MIBG HMR obtained using the CZT camera and that obtained using planar imaging. In contrast, the moderate concordance between cHMR_{reproj} and HMR_{planar} that we found using anterior reprojection images likely was related to the multipinhole collimation, which is responsible for a

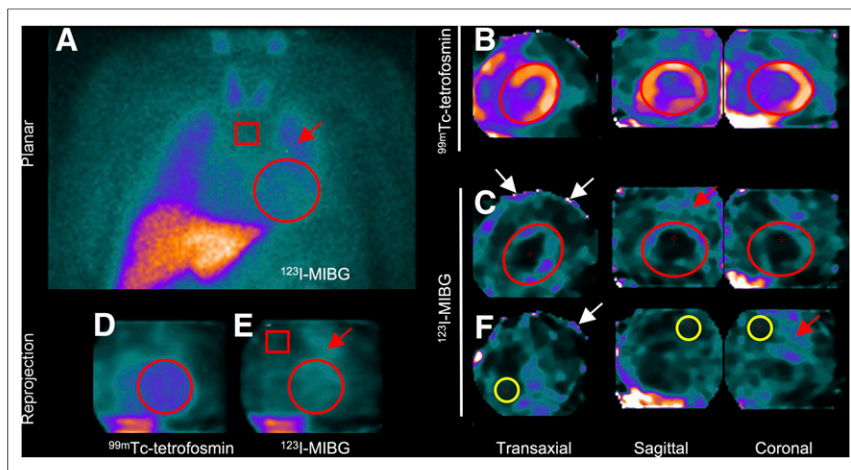


FIGURE 5. Patient 4 with ischemic heart failure (LVEF, 44%). HMRs calculated using conventional planar imaging ($\text{HMR}_{\text{planar}}$, 1.38) (A) and using DNM-530c with anterior reprojection images ($\text{HMR}_{\text{reproj}}$, 0.96) (E) and with transaxial reconstructed images ($\text{HMR}_{\text{transaxial}}$, 1.2) (C and F). $^{99\text{m}}\text{Tc}$ image allowed positioning on heart of ROI (D) or VOI (B) and was pasted onto ^{123}I image (E or C, respectively). (F) Mediastinum VOI on ^{123}I acquisition. $\text{HMR}_{\text{reproj}}$ and $\text{HMR}_{\text{transaxial}}$ were lower than $\text{HMR}_{\text{planar}}$. Lung activity (red arrows) and truncation artifacts (white arrows) were close to heart.

truncation artifact (31) that interferes with the mean counts of the myocardial ROI (Fig. 5) and for a larger nonuniformity with DNM-530c than with the Anger camera (31). This limitation was overcome through the use of reconstructed transaxial images instead of reprojection images for the measurement of corrected ^{123}I -MIBG HMR with DNM-530c in our population.

Dual-Isotope Acquisition

In the present study, we performed simultaneous dual-isotope DNM-530c acquisitions with $^{99\text{m}}\text{Tc}$ -tetrofosmin (358 ± 177 MBq) and ^{123}I -MIBG (191 ± 29 MBq). This dual-isotope acquisition allowed the simultaneous assessment of cardiac innervation and function. A previous phantom study demonstrated that under a simultaneous dual-isotope condition, the presence of ^{123}I did not have an impact on LVEF assessment within the $^{99\text{m}}\text{Tc}$ energy window for both dedicated CZT cameras (22). In addition, a simultaneous dual-isotope protocol provides a clearer $^{99\text{m}}\text{Tc}$ -tetrofosmin image and a perfect registration for defining the heart contours on the $^{99\text{m}}\text{Tc}$ -tetrofosmin image and therefore accurately measures cardiac ^{123}I -MIBG uptake (16). As shown in Figure 2, the amount of $^{99\text{m}}\text{Tc}$ activity had an impact on the $^{99\text{m}}\text{Tc}/^{123}\text{I}$ ratio but did not interfere with the energy resolution of the detector, modifying only the magnitude and not the width of the photopeak.

Finally, the acquisition of both SPECT and planar images using the Anger camera usually requires 30–45 min. In contrast, acquisition with CZT cameras usually requires 10 min; the latter is much more convenient in patients with heart failure.

Study Limitations

Because of the narrow field of view, the cardiac acquisition did not encompass the upper mediastinum. Consequently, the mediastinal ROI or VOI was positioned in the middle mediastinum on DNM-530c images, whereas the mediastinal ROI was set on the upper mediastinum when a conventional Anger camera was used (7). On the other hand, the size and placement (manual or automated) of the left ventricular ROI did not affect the delayed HMR

of ^{123}I -MIBG when conventional planar imaging was used (8). Therefore, further studies including a phantom-based cross-calibration are needed to standardize the placement of the mediastinal ROI or VOI using the different models of available cardiac CZT cameras (30). Finally, dual-isotope acquisition increases the radiation burden. In this retrospective study, the injected $^{99\text{m}}\text{Tc}$ -tetrofosmin activity was gradually decreased over time as it became clear that the CZT camera allowed the injection of small amounts of perfusion tracer without a compromise in image quality.

CONCLUSION

The present study demonstrated that determination of the late HMR of cardiac ^{123}I -MIBG uptake using dual-isotope (^{123}I and $^{99\text{m}}\text{Tc}$) acquisition on a multipinhole CZT camera (DNM-530c) is feasible in patients with heart failure. However, this determina-

tion should be performed using transaxial reconstructed images and a linear correction based on phantom data acquisitions.

DISCLOSURE

No potential conflict of interest relevant to this article was reported.

ACKNOWLEDGMENTS

We thank Amélie Lansiaux, Sylvie Petit, Mathilde Thélou, and the nuclear medicine technicians at Lille, France, for their technical assistance.

REFERENCES

- Merlet P, Valette H, Dubois-Randé JL, et al. Prognostic value of cardiac metaiodobenzylguanidine imaging in patients with heart failure. *J Nucl Med*. 1992;33:471–477.
- Nakata T, Miyamoto K, Doi A, et al. Cardiac death prediction and impaired cardiac sympathetic innervation assessed by MIBG in patients with failing and nonfailing hearts. *J Nucl Cardiol*. 1998;5:579–590.
- Merlet P, Benvenuti C, Moyse D, et al. Prognostic value of MIBG imaging in idiopathic dilated cardiomyopathy. *J Nucl Med*. 1999;40:917–923.
- Wakabayashi T, Nakata T, Hashimoto A, et al. Assessment of underlying etiology and cardiac sympathetic innervation to identify patients at high risk of cardiac death. *J Nucl Med*. 2001;42:1757–1767.
- Manrique A, Bernard M, Hitzel A, et al. Prognostic value of sympathetic innervation and cardiac asynchrony in dilated cardiomyopathy. *Eur J Nucl Med Mol Imaging*. 2008;35:2074–2081.
- Jacobson AF, Senior R, Cerqueira MD, et al. Myocardial iodine-123 meta-iodobenzylguanidine imaging and cardiac events in heart failure: results of the prospective ADMIRE-HF (Adreview Myocardial Imaging for Risk Evaluation in Heart Failure) study. *J Am Coll Cardiol*. 2010;55:2212–2221.
- Flotats A, Carrio I, Agostini D, et al. Proposal for standardization of ^{123}I -metaiodobenzylguanidine (MIBG) cardiac sympathetic imaging by the EANM Cardiovascular Committee and the European Council of Nuclear Cardiology. *Eur J Nucl Med Mol Imaging*. 2010;37:1802–1812.
- Veltman CE, Boogers MJ, Meinardi JE, et al. Reproducibility of planar ^{123}I -meta-iodobenzylguanidine (MIBG) myocardial scintigraphy in patients with heart failure. *Eur J Nucl Med Mol Imaging*. 2012;39:1599–1608.
- Sharir T, Ben-Haim S, Merzon K, et al. High-speed myocardial perfusion imaging initial clinical comparison with conventional dual detector Anger camera imaging. *JACC Cardiovasc Imaging*. 2008;1:156–163.

10. Herzog BA, Buechel RR, Katz R, et al. Nuclear myocardial perfusion imaging with a cadmium-zinc-telluride detector technique: optimized protocol for scan time reduction. *J Nucl Med*. 2010;51:46–51.
11. Imbert L, Poussier S, Franken PR, et al. Compared performance of high-sensitivity cameras dedicated to myocardial perfusion SPECT: a comprehensive analysis of phantom and human images. *J Nucl Med*. 2012;53:1897–1903.
12. Verger A, Djaballah W, Fourquet N, et al. Comparison between stress myocardial perfusion SPECT recorded with cadmium-zinc-telluride and Anger cameras in various study protocols. *Eur J Nucl Med Mol Imaging*. 2013;40:331–340.
13. Gimelli A, Liga R, Genovesi D, Giorgetti A, Kusch A, Marzullo P. Association between left ventricular regional sympathetic denervation and mechanical dys-synchrony in phase analysis: a cardiac CZT study. *Eur J Nucl Med Mol Imaging*. 2014;41:946–955.
14. Gimelli A, Liga R, Giorgetti A, Genovesi D, Marzullo P. Assessment of myocardial adrenergic innervation with a solid-state dedicated cardiac cadmium-zinc-telluride camera: first clinical experience. *Eur Heart J Cardiovasc Imaging*. 2014;15:575–585.
15. D'estanque E, Hedon C, Lattuca B, et al. Optimization of a simultaneous dual-isotope $^{201}\text{Tl}/^{123}\text{I}$ -MIBG myocardial SPECT imaging protocol with a CZT camera for trigger zone assessment after myocardial infarction for routine clinical settings: are delayed acquisition and scatter correction necessary? *J Nucl Cardiol*. May 25, 2016 [Epub ahead of print].
16. Bellevre D, Manrique A, Legallois D, et al. First determination of the heart-to-mediastinum ratio using cardiac dual isotope (^{123}I -MIBG/ $^{99\text{m}}\text{Tc}$ -tetrofosmin) CZT imaging in patients with heart failure: the ADRECARD study. *Eur J Nucl Med Mol Imaging*. 2015;42:1912–1919.
17. Bocher M, Blevis IM, Tsukerman L, Shrem Y, Kovalski G, Volokh L. A fast cardiac gamma camera with dynamic SPECT capabilities: design, system validation and future potential. *Eur J Nucl Med Mol Imaging*. 2010;37:1887–1902.
18. Bailliez A, Lairez O, Merlin C, et al. Left ventricular function assessment using 2 different cadmium-zinc-telluride cameras compared with a gamma-camera with cardiofocal collimators: dynamic cardiac phantom study and clinical validation. *J Nucl Med*. 2016;57:1370–1375.
19. Inoue Y, Suzuki A, Shirouzu I, et al. Effect of collimator choice on quantitative assessment of cardiac iodine 123 MIBG uptake. *J Nucl Cardiol*. 2003;10:623–632.
20. Verberne HJ, Feenstra C, de Jong WM, Somsen GA, van Eck-Smit BL, Busemann Sokole E. Influence of collimator choice and simulated clinical conditions on ^{123}I -MIBG heart/mediastinum ratios: a phantom study. *Eur J Nucl Med Mol Imaging*. 2005;32:1100–1107.
21. Blaire T, Bailliez A, Ben Bouallegue F, Bellevre D, Agostini D, Manrique A. First assessment of simultaneous dual isotope ($^{123}\text{I}/^{99\text{m}}\text{Tc}$) cardiac SPECT on two different CZT cameras: a phantom study. *J Nucl Cardiol*. March 8, 2017 [Epub ahead of print].
22. Blaire T, Bailliez A, Bouallegue FB, Bellevre D, Agostini D, Manrique A. Left ventricular function assessment using $^{123}\text{I}/^{99\text{m}}\text{Tc}$ dual-isotope acquisition with two semi-conductor cadmium-zinc-telluride (CZT) cameras: a gated cardiac phantom study. *EJNMMI Phys*. 2016;3:27.
23. Inoue Y, Abe Y, Itoh Y, et al. Acquisition protocols and correction methods for estimation of the heart-to-mediastinum ratio in ^{123}I -metaiodobenzylguanidine cardiac sympathetic imaging. *J Nucl Med*. 2013;54:707–713.
24. Lin LI. A concordance correlation coefficient to evaluate reproducibility. *Biometrics*. 1989;45:255–268.
25. Bland JM, Altman DG. Statistical methods for assessing agreement between two methods of clinical measurement. *Lancet*. 1986;1:307–310.
26. Erlandsson K, Kacperski K, van Gramberg D, Hutton BF. Performance evaluation of D-SPECT: a novel SPECT system for nuclear cardiology. *Phys Med Biol*. 2009;54:2635–2649.
27. Gambhir SS, Berman DS, Ziffer J, et al. A novel high-sensitivity rapid-acquisition single-photon cardiac imaging camera. *J Nucl Med*. 2009;50:635–643.
28. Nakajima K, Okuda K, Matsuo S, et al. Standardization of metaiodobenzylguanidine heart to mediastinum ratio using a calibration phantom: effects of correction on normal databases and a multicentre study. *Eur J Nucl Med Mol Imaging*. 2012;39:113–119.
29. Nakajima K, Okuda K, Yoshimura M, et al. Multicenter cross-calibration of I-123 metaiodobenzylguanidine heart-to-mediastinum ratios to overcome camera-collimator variations. *J Nucl Cardiol*. 2014;21:970–978.
30. Verschure DO, Poel E, Nakajima K, et al. A European myocardial ^{123}I -mIBG cross-calibration phantom study. *J Nucl Cardiol*. January 24, 2017 [Epub ahead of print].
31. Takahashi Y, Miyagawa M, Nishiyama Y, Ishimura H, Mochizuki T. Performance of a semiconductor SPECT system: comparison with a conventional Anger-type SPECT instrument. *Ann Nucl Med*. 2013;27:11–16.



The Journal of
NUCLEAR MEDICINE

Determination of the Heart-to-Mediastinum Ratio of ^{123}I -MIBG Uptake Using Dual-Isotope (^{123}I -MIBG/ $^{99\text{m}}\text{Tc}$ -Tetrofosmin) Multipinhole Cadmium-Zinc-Telluride SPECT in Patients with Heart Failure

Tanguy Blaire, Alban Bailliez, Fayçal Ben Bouallegue, Dimitri Bellevre, Denis Agostini and Alain Manrique

J Nucl Med. 2018;59:251-258.

Published online: June 23, 2017.

Doi: 10.2967/jnumed.117.194373


This article and updated information are available at:
<http://jnm.snmjournals.org/content/59/2/251>

Information about reproducing figures, tables, or other portions of this article can be found online at:
<http://jnm.snmjournals.org/site/misc/permission.xhtml>

Information about subscriptions to JNM can be found at:
<http://jnm.snmjournals.org/site/subscriptions/online.xhtml>

The Journal of Nuclear Medicine is published monthly.
SNMMI | Society of Nuclear Medicine and Molecular Imaging
1850 Samuel Morse Drive, Reston, VA 20190.
(Print ISSN: 0161-5505, Online ISSN: 2159-662X)

© Copyright 2018 SNMMI; all rights reserved.

 SOCIETY OF
NUCLEAR MEDICINE
AND MOLECULAR IMAGING